Journal of Hydrology 583 (2020) 124581

Contents lists available at ScienceDirect

Journal of Hydrology

journal homepage: www.elsevier.com/locate/jhydrol

Research papers

Modeling the impacts of urbanization on watershed-scale gross primary productivity and tradeoffs with water yield across the conterminous United States

Cheng Li[a,b], Ge Sun[c,*], Erika Cohen[c], Yindan Zhang[d,e,f], Jingfeng Xiao[g], Steven G. McNulty[c], Ross K. Meentemeyer[d,e]

[a] Guangdong Key Laboratory of Integrated Agro-environmental Pollution Control and Management, Guangdong Institute of Eco-Environmental Science & Technology, Guangzhou 510650, China
[b] National-Regional Joint Engineering Research Center for Soil Pollution Control and Remediation in South China, Guangzhou 510650, China
[c] Eastern Forest Environment Threat Assessment Center, USDA Forest Service, Research Triangle Park, NC 27709, USA
[d] Center for Geospatial Analytics, North Carolina State University, Raleigh, NC 27606, USA
[e] Department of Forestry and Environmental Resources, North Carolina State University, Raleigh, NC 27606, USA
[f] College of Earth and Environmental Sciences, Lanzhou University, Lanzhou 730000, China
[g] Earth Systems Research Center, Institute for the Study of Earth, Oceans, and Space, University of New Hampshire, Durham, NH 03824, USA

ARTICLE INFO

This manuscript was handled by G. Syme, Editor-in-Chief, with the assistance of Bellie Sivakumar, Associate Editor

Keywords:
Carbon balance
Water balance
Urban sprawl
Ecosystem model
Causal analysis

ABSTRACT

The objective of this study was to examine the impacts of urbanization on gross primary productivity (GPP) and the interactions between carbon and water fluxes, including precipitation, evapotranspiration (ET), and water yield (Q). A water-centric ecosystem model, Water Supply Stress Index model (WaSSI) that operates at the 12-digit (81,900 watersheds) Hydrologic Unit Code (HUC) scale for the conterminous United States (CONUS) during 2000–2010, 2000–2050, and 2000–2100 was used. Linear regression and causal-based models were then applied to identify key factors controlling urbanization impact on GPP. Simulations of GPP patterns compared favorably with a global, 0.05-degree product of solar-induced chlorophyll fluorescence (SIF). We found that total CONUS GPP declined from 8.68 Pg C yr^{-1} in 2000, to 8.54 Pg C yr^{-1} in 2010, to 8.36 Pg C yr^{-1} in 2050, and to 8.13 Pg C yr^{-1} in 2100. Total GPP decreased from 6.81 Pg C yr^{-1} to 6.26 Pg C yr^{-1} for those watersheds affected by urbanization (~55,000). Total CONUS Q increased from 2.03 × 10^6 million m^3 yr^{-1} in 2000, to 2.04 × 10^6 million m^3 yr^{-1} in 2010, to 2.06 × 10^6 million m^3 yr^{-1} in 2050, and 2.09 × 10^6 million m^3 yr^{-1} in 2100, while Q increased from 1.68 × 10^6 million m^3 yr^{-1} to 1.74 × 10^6 million m^3 yr^{-1} for urbanized watersheds alone (~55,000). Although total CONUS ΔGPP was less than 0.55 Pg C yr^{-1}, or < 8%, large changes (ΔGPP > 300 g C m^{-2} yr^{-1}) were found in 245, 1984, and 5655 of the 81,900 watersheds by 2010, 2050 and 2100, respectively. Overall, the impacts of urbanization on GPP in the CONUS were influenced by background climate, previous land cover characteristics, and the magnitudes of land use change. Effective integrated watershed management that attempts to minimize the negative ecological and environmental impacts of urbanization must consider regional hydrologic differences and fit local climatic and watershed conditions.

1. Introduction

Urbanized land area accounts for a tiny portion of the earth's terrestrial surface (< 3%) (Liu et al., 2014), but it contributes to 60% of residential water use, 78% of carbon emission, and 80% of wood consumption for industrial purposes (Grimm et al., 2008). Urbanization substantially reduces vegetation cover as urban areas are typically dominated by impervious surfaces. Rapid urbanization has significantly altered ecosystem functions (Grimm et al., 2008; Wu, 2014) and threatened ecosystem services such as clean water supply (Sun et al., 2015a), climate regulation (Hao et al., 2018), and carbon sequestration (Cui et al., 2017).

Gross primary production (GPP), one of the key ecosystem services (Sun et al., 2011b), represents the total fixation of carbon by vegetation through the photosynthesis process (Chapin et al., 2002; Beer et al., 2010). GPP plays a critical role in both the terrestrial ecosystem and

* Corresponding author.
E-mail address: Ge.Sun@USDA.Gov (G. Sun).

https://doi.org/10.1016/j.jhydrol.2020.124581

Available online 25 January 2020
0022-1694/ Published by Elsevier B.V.

global carbon cycles (Cui et al., 2017; Sun et al., 2018). As estimated by Xiao et al. (2010), the GPP of the conterminous U.S. was between 6.91 and 7.33 Pg C yr^{-1}. Extreme climate events and disturbances such as drought and fire reduced annual GPP at regionals scales (Xiao et al., 2011; Sun et al., 2015c; Xiao et al., 2016). Permanent vegetation removal due to urbanization, particularly the transformation from rural land uses of agriculture or forestry to urban land uses characterized by large impervious surfaces might also reduce annual GPP (Sun and Lockaby, 2012). As evidenced, conversions of croplands or grasslands to urban development dramatically reduced ecosystems' carbon fixation ability up to 50% (Liu et al., 2018b; Nuarsa et al., 2018).

Few studies have quantified the impacts of urbanization on GPP (Zhao et al., 2007). Existing results are mixed due to the complexity of urbanization and diverse ecosystem responses to urbanization across space. In general, urban land development has negative effects on GPP at multiple scales, mainly due to the decrease in vegetation coverage (McHale et al., 2017; Nuarsa et al., 2018; Seto et al., 2012; Sun et al., 2019). However, positive effects were also observed in some regions previously dominated by crops or deserts (Buyantuyev and Wu, 2009; Zhao et al., 2007). As indicated by Miller et al. (2018), the urbanization effects vary by biome. Urban area growth and vegetation change may collectively cause an increase, a decrease or no change in GPP of urban ecosystems through time (Cui et al., 2017). Our understanding of the impacts of urbanization on the terrestrial carbon cycle is still limited (Churkina, 2008; Romero-Lankao et al., 2014).

Accurate *in situ* measurements of GPP in urban ecosystems are rare due to the complex urban landscape. Remote sensing and simulation models have been used to estimate GPP response to human disturbances in various regions (Gitelson et al., 2014; Jung et al., 2017; Monteith, 1972; Potter et al., 1993; Running and Zhao, 2015; Sun et al., 2011b; Sun et al., 2019). Sun et al. (2019) categorized these models into four types: 1) biophysical process-based, such as BESS (Breathing Earth System Simulator) and BEPS (Boreal Ecosystem Productivity Simulator), 2) vegetation-indexed based, such as VIM (Vegetation-indices Model) and GRM (Greenness-Radiation Model), 3) light-use-efficiency based such as CASA (Carnegie-Ames-Stanford Approach) and EC-LUE (Eddy Covariance Light-Use Efficiency), and 4) machine-learning-based models such as piecewise regression models, artificial neural network, and random forest. However, urban areas were usually excluded in regional studies due to the lack of parameters for urban ecosystems (e.g., vegetation cover and type, water and light use efficiency) and the heterogeneity of urban landscape (e.g., impervious surface, buildings, vegetation) and management (Cui et al., 2017; Miller et al., 2018).

Carbon and water cycles are tightly coupled (Sun et al., 2011b; Sun et al., 2019; Wu et al., 2016) as demonstrated by the close GPP and evapotranspiration (ET) relationships (Law et al., 2002; Lei et al., 2014; Zhang et al., 2016a; Proietti et al., 2019). ET is a key component of the hydrological cycle, and a critical linkage to ecosystem carbon fluxes (Sun et al., 2011a). Urbanization and climate change affect watershed hydrologic and carbon fluxes mainly through altering the ET processes (Sun and Lockaby, 2012). Indeed, the connection between ET and GPP has been successfully used to estimate ecosystem carbon fluxes (Beer et al., 2007; Sun et al., 2011b) or water flux (Zhang et al., 2016a) at a national scale. The present study uses such type of water-centric ecosystem model (Water Supply Stress Index, WaSSI) (Sun et al., 2011b) to estimate carbon fluxes from water fluxes. The WaSSI model has been widely used to quantify effects of urbanization on water fluxes (Caldwell et al., 2012) and the effects of drought on GPP and water yield (Sun et al., 2015b; Sun et al. 2015c; Duan et al., 2016). We are not aware of previous studies on the impacts of urbanization on GPP at a national level in the U.S.

The overall goal of this study was to improve our understanding of the coupled changes in water and carbon fluxes in the next 100 years under a projected urbanization scenario across the U.S. Such knowledge is essential for managing ecosystems (Mo et al., 2018) and mitigating environmental problems caused by urbanization (Finzi et al., 2011) at a national level. The objective of this simulation study was to quantify the responses of watershed GPP, ET, and water yield to urbanization using an integrated model. We examined changes in carbon and water under various climate and land cover characteristics, and land use and land cover changes (LULCC) through time at 12-digit, 8-digit, and 2-digit Hydrologic Unit Code (HUC) watershed scales. The U.S. watersheds are classified using several hierarchy levels, where lower hierarchy (e.g. 12-digit) are nested within the higher hierarchy levels (e.g. 8-digit, 2-digit).

We hypothesize that 'responses of GPP to urbanization are not created equal.' Specifically, our hypotheses are: 1) The decreases of GPP are due to both the urban area growth and reduction in evapotranspiration (Hypothesis 1-H1), and 2) The magnitude of GPP change varies with background climate (i.e., high precipitation vs low precipitation), previous LULC (e.g. grassland, shrubland, or barren with low biomass and forest with high biomass), and the magnitude of LULCC (Hypothesis 2-H2).

2. Materials and methods

2.1. Water supply stress Index (WaSSI) model

2.1.1. WaSSI model description

The WaSSI model (Sun et al., 2011b; Caldwell et al., 2012) was initially designed to estimate water and carbon balances and to determine the watershed water stress and ecosystem responses to changes in climate, land use and land cover, and human water demand. The model simulates key ecohydrologic and carbon fluxes including water yield, ET, and GPP, and Net Ecosystem Productivity (NEP). The model has been tested in the U.S., Australia, China, Mexico, and African countries for assessing forest management and climate change effects on ecosystem services (Bagstad et al., 2018; Duan et al., 2016; Liu et al., 2018a; Sun et al., 2011b). For example, Duan et al. (2016) and Sun et al. (2015b, 2015c) evaluated the impacts of climate change and drought on GPP and water yield in the U.S. National Forests.

For water cycle modeling, the WaSSI model simulates surface runoff, baseflow, ET, infiltration, soil moisture storage, and snowpack and melting by integrating built-in algorithms from Sacramento Soil Moisture Accounting Model (SAC-SMA) and ancillary data (Table 1; Sun et al., 2011b). The core of the WaSSI model is an ET model that empirically estimates ET as a function of PET, leaf area index (LAI), and water availability (i.e., precipitation, soil moisture) (Sun et al., 2011a).

As a water-centric ecosystem model, WaSSI estimates carbon balance from water fluxes using a water use efficiency (WUE) approach (Sun et al., 2011b). GPP is determined as a function of ET and biome-specific WUE that was derived from global eddy flux data (GPP = WUE*ET) (Sun et al., 2011b). For urban ecosystems, in lieu of a reliable WUE parameter, WUE for savanna ecosystem type reported in Sun et al. (2011b) was used as a surrogate for vegetated urban areas. GPP for impervious areas for any LULC type was assumed to be zero.

The WaSSI model simulates monthly water and carbon balance for each of the 10 land cover types used in the model and results are aggregated to the watershed level of 12-digit Hydrologic Unit Code (HUC12) by an area-weighted average approach (Caldwell et al., 2012; Sun et al., 2011b). Model outputs of ET, water yield, and GPP were summarized to the annual level. The 18 HUC2, 2,100 HUC8, and about 81, 900 HUC12 level watersheds are defined by the Watershed Boundary Dataset (Sun et al., 2011b). A few HUC12 watersheds that represent coastal watersheds with missing land use data or waterbodies were excluded from this analysis. More detailed descriptions and applications for the WaSSI model can be found in Sun et al. (2011b), Caldwell et al. (2012), and Sun et al. (2015b, c).

2.1.2. WaSSI model input datasets

This study estimated GPP responses to urbanization in recent (2000, 2010), middle (2050), and long term (2100) time frame. WaSSI model

Table 1
Summary of databases used for WaSSI model parameterization and validation of outputs.

Data	Temporal and spatial resolution	Data sources
Land cover and land use, impervious surface	2000, 2010, 2050, 2100; 90 m × 90 m	EPA; ICLUS version 2.1 (U.S. EPA, 2017); ICLUS V2.1 uses a new spatial allocation model to calculate demand for each land use class in relation to population density. It projected land use and impervious surface products for the year 2050 and 2100 with global socioeconomic scenarios (SSPs; SSP5 scenarios chosen in this study).
Historic climate (monthly precipitation, temperature)	1961–2010; 4 km × 4 km	Parameter-elevation Regressions on Independent Slopes Model (PRISM) (http://www.prism.oregonstate.ed; Caldwell et al., 2012)
Leaf Area Index (LAI)	2000–2012; 1 km × 1 km	Moderate Resolution Imaging Spectroradiometer (MODIS) (Zhao et al., 2005)
11 Soil parameters	For SAC-SMA soil model; 1 km × 1 km	State Soil Geographic Database (STATSGO) (https://water.usgs.gov/GIS/metadata/usgswrd/XML/muid.xml
Water use efficiency (WUE) parameters	Annual by biome	Derived from eddy flux sites (Sun et al., 2011b)
Upscaled GPP product for model validation	1 km × 1 km; 8-day interval	EC-MOD GPP product for North America (Xiao et al., 2014b)
Satellite-derived solar-induced chlorophyll fluorescence for model validation of GPP	0.05° × 0.05° grid; 8-day interval	Global, OCO2- based SIF product (GOSIF) (Li and Xiao, 2019)
WaSSI model outputs: ET, water yield, and GPP	Monthly, annual	WaSSI model (Sun et al., 2011b)

requires five categories of input datasets (Table 1) including historical climate of precipitation and air temperature (1961–2010), each of ten land cover fraction and impervious surface fraction within each land cover types in the four studied periods, STATSGO-based soil parameters, and mean monthly LAI data (2000–2012) by each land cover type (Caldwell et al., 2012; Sun et al., 2011b). The impervious surface fraction or LAI for each land cover type was derived by overlaying the impervious surface layer or MODIS LAI layer with the land cover layer. The ten LULC categories include deciduous forest, evergreen forest, mixed forest, shrubland, grassland, cropland, waterbody, wetland, urban, and barren land. However, because there is only one category for forest in the ICLUS datasets, we divided the forest fraction equally and reconstructed three forest covers with the same LAI value. Simulations for 2010, 2050, and 2100 were compared to those for the baseline year 2000 to determine the impacts of urbanization on GPP and water yield.

This study does not intend to address ecosystem responses to climate change, and therefore a static historical climate (1961–2010) was used for all the simulations. Similarly, we assumed that LAI would not change over time, and the mean LAI dataset (2000–2012) was used for all simulations.

2.1.3. WaSSI model validation

The WaSSI model has been applied worldwide and well-validated with hydrologic measurements (US: Caldwell et al., 2012; Sun et al., 2011b; Sun et al., 2016; China: Liu et al., 2013; Australia: Liu et al., 2018a; Rwanda: Bagstad et al., 2018). Therefore, this study focused on GPP validation using two data sources to ensure the quality of GPP estimates and their potential bias for urban ecosystems.

Because most remote-sensing based GPP products do not include urban areas, they are not appropriate for model validation purposes. Thus, we validated WaSSI estimates for GPP using a proxy for GPP, the Orbiting Carbon Observatory-2 (OCO-2) based solar-induced chlorophyll fluorescence (GOSIF) products. Studies have found that SIF was strongly correlated with GPP measured at flux sites across a wide variety of biomes (Li et al., 2018c). In this study, we used a global, OCO-2 based SIF product (GOSIF) that consists of 8-day, gridded SIF estimates over the period 2000–2018 (Li and Xiao, 2019). GOSIF was derived from three categories of datasets, including SIF soundings from the OCO-2, data streams from the Moderate Resolution Imaging Spectroradiometer (MODIS), and meteorological reanalysis data. The dataset is proved to be highly correlated with flux tower-based GPP estimates (Li and Xiao, 2019).

As mentioned earlier (Section 2.1.2), the ICLUS datasets had only one land-use type for forest. Therefore, we used the 2006 National Land Cover Database (NLCD) for GPP validation. The original 16 land cover types for NLCD were lumped into ten types to meet the requirements of the WaSSI model. To be consistent with the NLCD products, we used the impervious surface fraction from ICLUS V2.1 product, and LAI data products in the same year of 2006 (Zhao et al., 2005). We aggregated the SIF data from the GOSIF product (Li and Xiao, 2019) to both HUC12 and HUC8 watershed levels to compare the mean SIF values for 2000–2010 to the WaSSI GPP estimates in 2006. Similarly, we compared an upscaled GPP product, EC-MOD (Xiao et al., 2014b) with the SIF product (Li and Xiao, 2019) at both HUC12 and HUC8 watershed levels. The EC-MOD GPP product was derived from eddy covariance, MODIS, and meteorological reanalysis data using a data-driven approach (Xiao et al., 2008; Xiao et al., 2010) and consists of 8-day, 1 km-resolution GPP estimates for North America over the period 2000–2012. This comparison only applies to non-urban areas because urban lands were masked out in the EC-MOD GPP product (Xiao et al., 2010).

2.2. Statistical analyses

2.2.1. Selection of independent variables

Based on our hypotheses and previous literature (As-syakur et al., 2010; Awal et al., 2010; Cui et al., 2017; Miller et al., 2018; Nuarsa et al., 2018), we chose 17 independent variables to examine their influences on the urbanization impacts on GPP. These 17 variables were categorized into three groups: 1) background climate including precipitation (PPT) and temperature (TEMP), 2) previous land cover characteristics expressed as the area fraction of impervious surface and seven land cover types (i.e., forest, cropland, shrubland, grassland, wetland, waterbody, and urban) within a watershed of the baseline year 2000, and 3) land use and land cover change (LULCC) expressed as the absolute changes of a particular land cover fraction within a watershed from 2000 to 2010, 2050, and 2100. All the previous land cover characteristics and LULC changes were denoted by the first three or four letters of the land cover type with the source year or time period attached. For example, forest fraction in 2000 and its changes from 2000 to 2050 were denoted by For00 and For0050, respectively. In addition, all the variables were standardized (i.e., mean 0, standard deviation of 1) to eliminate the effects of dimensions for further analyses.

2.2.2. Interactions between carbon and water fluxes

We compared both the spatiotemporal changes of gross primary production (GPP), evapotranspiration (ET), and water yield (Q) for 48,000–55,000 HUC12 watersheds impacted by urbanization during 2000–2010, 2000–2050, and 2000–2100 to assess the interactions of carbon and water fluxes. In addition, the linear regression of the changes in GPP to changes in ET during 2000–2010, 2000–2050 and

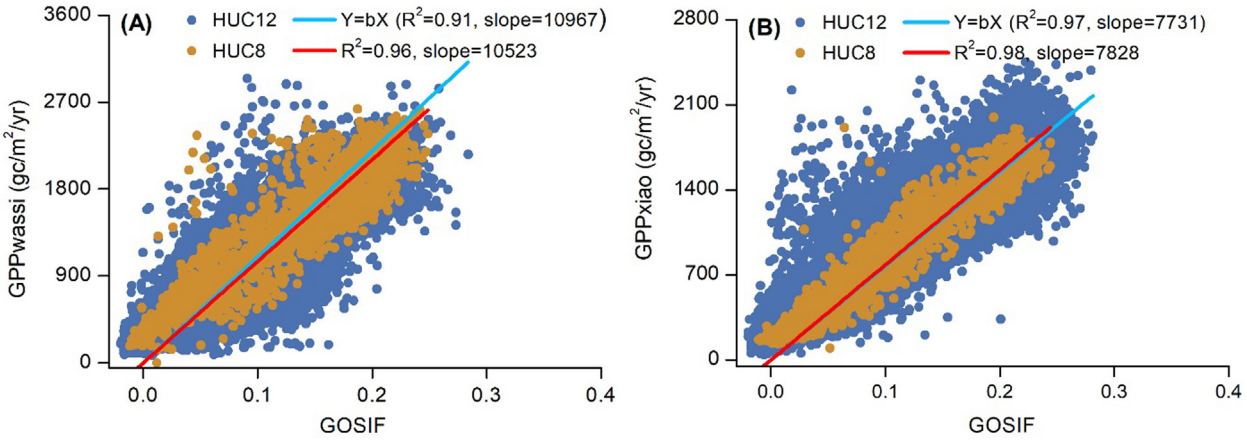

Fig. 1. Scatter plot to show relationship between estimated gross primary productivity (GPP) in 2006 by the WaSSI model and mean OCO2- based solar-induced chlorophyll fluorescence (GOSIF) from 2000 to 2012 (A), and (B) estimated GPP by Xiao et al. (2008, 2010, 2011) and GOSIF from 2008 to 2012.

2000–2100 at both HUC12 and HUC8 scales were further conducted to quantify their interactions.

2.2.3. The impacts of urbanization on GPP by linear regression analyses

Linear regression analyses were used to examine GPP responses to urbanization and associated hydrological change, including ET (testing Hypothesis#1-H1). Standardized stepwise regression was used to explore the relationships among GPP, background climate, previous land cover characteristics, and LULCC to test Hypothesis #2 (H2). Prior to the stepwise regression analysis, collinearity analysis was conducted to remove the independent variables using thresholds of Variance Inflation Factor (VIF) and Minimum Tolerance Values large than 5 or less than 0.2, respectively. The importance of independent variables in explaining GPP variations was ranked by the stepwise regression coefficients because the independent variables were standardized.

2.2.4. The impacts of urbanization on GPP by a causal model

We further used a general causal model, the Directed Acyclic Graph (DAG) is Absent (IDA), to determine the causation relationship between the change in GPP and the selected environmental factors (Kalisch et al., 2012) because correlations do not necessarily mean causation. There are a few established methods, such as the Structural Equation Model (SEM), that can be used to identify the causal effect between variables from the observational data (Grace, 2006). However, such methods are usually based on an unrealistic assumption that the potential causal relationships between variables are known (Maathuis et al., 2010). Unlike the previous mathematical models, IDA simulates an intervention process of the system and predicts the causal effects of the interventions without such prior causal knowledge (Maathuis et al., 2010; Pearl, 1995). IDA has been well validated for a biological system (Maathuis et al., 2010) and has been applied in many other research fields such as soil contamination (Liu et al., 2017; Wang et al., 2018b) and social science (Morgan, 2013).

The causal structure identification and causal effect estimation are two modules for IDA and are computed with either the Peter-Clark (PC) (Pearl, 1995) or Pearl's do-calculus algorithm (Pearl, 2003). The causal structure derived by PC algorithms is explicitly characterized by a network with nodes (representing dependent and independent variables) and edges (direct causals) called a Directed Acyclic Graph (DAG) (Pearl, 2003; Wang et al., 2018b). The PC algorithms initially identify an undirected graph with nodes and edges, and then convert it to a complete partially directed acyclic graph (CPDAG) by d-separation (Pearl, 2003; Wang et al., 2018b). The CPDAG is in the form of nodes and both directional and unidirectional edges based on the conditional independence tests (e.g., gauss CI Test) at a certain significance level (Kalisch and Bühlmann, 2007; Kalisch et al., 2012; Pearl, 2003; Wang et al., 2018b). The edges are deleted if conditionally independent. Otherwise they are retained. The PC algorithm creates one CPDAG and the equivalence class of the DAGs (with the same skeleton, v-structures, and equally valid conditional independence information) to characterize the causal structure. The arrows might be in different directions in different DAGs in the equivalence class, meaning that the possible causal effect is not a unique value but a set of causes. The Pearl's do-calculus algorithm was conducted on each equivalence class of the DAGs by either global or local method. A multiset of possible casual values was estimated, and we used the lower bound of the causal effects as the final results. The PCalg package for R (version: R3.4.2) was used to develop IDA (Kalisch et al., 2012).

3. Results

3.1. Validation of modeled GPP

The aggregated mean watershed-scale EC-MOD GPP (Xiao et al., 2008; Xiao et al., 2011; Xiao et al., 2010) correlated well with GOSIF (Li and Xiao, 2019) at both HUC12 and HUC8 watershed scales (urban area not included) (R^2 = 0.97–0.98, $p < 0.05$; Fig. 1). This demonstrates the validity of GOSIF as a proxy of GPP at the watershed scale. We further compared the mean GPP modeled by WaSSI with the GOSIF product, both including urban areas. As indicated by Fig. 1, our modeled mean GPP was also well-collated with mean GOSIF at both HUC12 and HUC8 spatial scales (R^2 = 0.91–0.96, $p < 0.05$), confirming the strength of the WaSSI model in modeling GPP for all LULC.

3.2. Change in urban areas

Among the 81,900 HUC12 watersheds, the mean fraction for urban areas ranged from 11.7% to 20.6% in 2000, 2010, 2050, and 2100. About 30%-40% of the watersheds did not show change in urbanization (Fig. 2). We focused on the 48,000–55,000 watersheds experiencing obvious changes in urban growth at both the HUC12 and HUC8 watershed scales. Among the 48,000–55,0000 watersheds experiencing urban expansion, the urban growth rate increased dramatically over time. The mean absolute change in the urban area fraction was 0.05, 0.08 and 0.13 during 2000–2010, 2000–2050 and 2000–2100, respectively (Fig. 1-D). The number of watersheds with an increase in urban area fraction greater than 0.5 accelerated from 201 during the 2000–2010 period, to 777 during 2000–2050, and to 2628 during 2000–2100 (Fig. 2-B). Similarly, mean relative changes in urban area were 148%, 351% and 712% during 2000–2010, 2000–2050, and 2000–2100, respectively (Fig. 2-E). The number of watersheds with a relative urban area increase of greater than 300% increased from 3933

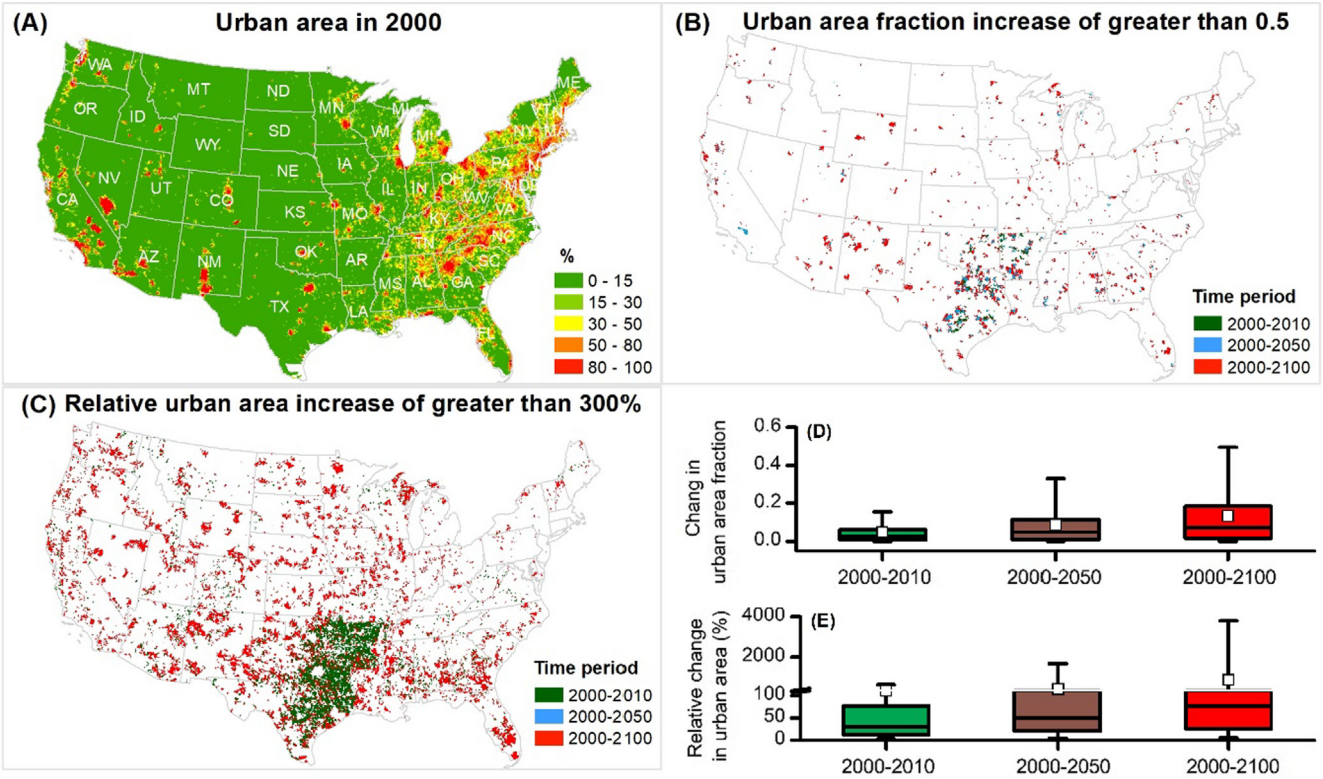

Fig. 2. The percentage of urban area in 2000 (A), watersheds with urban area fraction increased by greater than 0.5 (B), watersheds with relative urban area increased by greater than 300% (C) and box-charts of change in urban fraction and relative change in urban area (D) during 2000–2010, 2000–2050 and 2000–2100 at 12-digit Hydrologic Unit Code (HUC12) watershed scale. The square is the mean value of the change, while the solid line is the median. The lower and upper whisker represents the 5th percentile and 95th percentile of the change, respectively.

during 2000–2010, to 7830 during 2000–2050, and to 11,963 during 2000–2100 (Fig. 2-B). In addition, the CONUS urban area growth was pronounced in the southern U.S. for areas such as Oklahoma (OK), Arkansas (AR), Louisianan (LA) and Texas (TX) (Fig. 2-B, 2-C).

3.3. Modeled change in GPP

Among the 81,900 watersheds, total gross carbon uptake of the CONUS was estimated to be 8.68, 8.54, 8.36 and 8.13 Pg C yr^{-1} in 2000, 2010, 2050 and 2100, respectively. This represented as a decrease in GPP of 1.61%, 3.69%, and 6.34% in 2010, 2050 and 2100, respectively. The gross carbon uptake for only urbanized watersheds (~55,000) decreased from GPP for the 6.81 Pg C yr^{-1} in 2000, to 6.67 Pg C yr^{-1} in 2010, to 6.49 Pg C yr^{-1} in 2050, and 6.26 Pg C yr^{-1} in 2100, with the decrease of 2.06%, 4.70%, and 8.08% in 2010, 2050 and 2100, respectively. Although the impact of future urbanization on mean GPP (ΔGPP) was small at the national level, large changes (ΔGPP > 300 g C m^{-2} yr^{-1}) were found in 245, 1984, and 5655 of the 81,900 watersheds by 2010, 2050 and 2100, respectively. In contrast, the total water yield (Q) at the CONUS level increased from 2.03×10^6 million m^3 yr^{-1} in 2000, to 2.04×10^6 million m^3 yr^{-1} in 2010, to 2.06×10^{12} million m^3 yr^{-1} in 2050, and 2.09×10^{12} million m^3 yr^{-1} in 2100; while increased from 1.68×10^6 to 1.74×10^6 for only urbanized watersheds (~55,000). The gross carbon uptake ability of the CONUS ecosystems decreased through time and varied spatially among the 18 water resource regions (WRRs). For example, the top four areas with the greatest decreased GPP during 2000–2050 were WRR03 (Mean ± Standard Deviation, $11.5 \pm 15.6 \times 10^9$ g C yr^{-1}), WRR06 ($8.8 \pm 9.6 \times 10^9$ g C yr^{-1}), WRR08 ($11.6 \pm 16.5 \times 10^9$ g C yr^{-1}) and WRR11 ($10.3 \pm 15.9 \times 10^9$ g C yr^{-1}) in the southeastern U.S. (Fig. 3). These regions are wet regions with high ET due to high precipitation and available energy. In contrast to a decrease in GPP, these WRRs showed an increase in Q. The increase in total water yield volume for WRR03, WRR06, WRR18 and WRR12 during 2000–2050 was $10.2 \pm 19.8 \times 10^5$ m^3, $6.8 \pm 9.8 \times 10^5$ m^3, $6.6 \pm 13.1 \times 10^5$ m^3, and $9.1 \pm 21.2 \times 10^5$ m^3, respectively due to reductions in ET (Fig. 3). Changes in GPP and Q showed similar contrasting pattern during other two time periods, i.e., 2000–2010 and 2000–2100 (not shown).

The modeled decrease in GPP from 2000 to 2100 varied greatly over the US (Figs. 4, S1). For watersheds projected to increase in urban area (total 48,000–55,000), the mean and standard deviations of annual decrease in GPP were -31.0 ± 45.3, -67.0 ± 97.3 and -108.6 ± 151.1 g C m^{-2} yr^{-1} during 2000–2010, 2000–2050 and 2000–2100, respectively (Fig. 5-A). Similarly, the absolute change in GPP was most pronounced in the southeastern U.S., and coincided with high GPP values of the baseline year 2000. However, the mean relative change in GPP was most obvious in the dry regions, ranging from −8.1% to −2.3% (Figs. 5-B, S1).

3.4. Interactions between carbon and water fluxes

By model design, the carbon (GPP) and water fluxes (ET) are inherently coupled, and thus GPP, ET and Q patterns followed each other closely. Among the 48,000–55,000 watersheds with urbanization, GPP and ET generally decreased while Q increased during the three time periods (Fig. 6). The top four regions in change in Q (ΔQ) overlapped with regions with decrease in carbon uptake (WRR03, WRR06, WRR08, and WRR12; Fig. 3). Similarly, the absolute change in ET was most obvious in eastern U.S. with mean annual changes ranging from −2.8 to −11.7 mm during the three time periods (Figs. 7, 8-A). However, the mean relative change in ET ranged from −0.5% to −2.1% with high values mainly located in western U.S. (Fig. 8-B, S2). Although modeled GPP was estimated to be directly proportional to ET by biome in this study, the relationship between changes in GPP and changes in ET rates

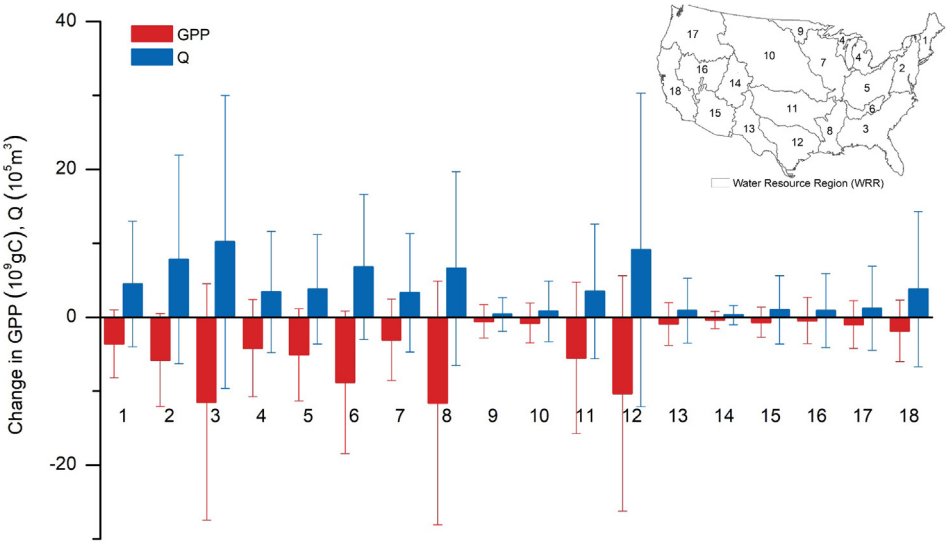

Fig. 3. Simulated effects of urbanization on gross primary productivity (GPP) and water yield (Q) by 18 waters resource regions (WRR) from 2000 to 2050.

were not linear at the watershed level as indicated by the low adjusted R^2 values at both the HUC12 and HUC8 watershed scales during the three time periods (Fig. 9).

3.5. Relationships between GPP and urbanization

3.5.1. GPP responses to urbanization determined by linear regression models

The change in GPP (ΔGPP) was linearly correlated with the increase in urban areas at both watershed scales when data were pooled for all time periods (R^2 = 0.81–0.94, $p < 0.05$; Figs. 10, S3). However, the impacts of urbanization on ΔGPP varied greatly among watersheds that have different watershed size, baseline land cover, background climate, and magnitude of land cover change (Figs. 11–13, S4–S6). The ΔGPP for watersheds at the HUC8 scale is larger than that at the HUC12 scale. The ΔGPP data for HUC12 watersheds were more scattered, indicating a higher variability than the larger HUC8 watersheds. The differences at the two spatial levels suggested that the urbanization effects became more variable as the watershed sizes decreased. ΔGPP values were generally high for the watersheds previously dominated by wetland, cropland, and forest and urban land compared with those of grassland and shrubland, as indicated by the steeper slopes of the relationships (Fig. 11, S4). Similarly, the mean GPP for watersheds in wet regions was more sensitive (R^2 = 0.90–0.94; regression model

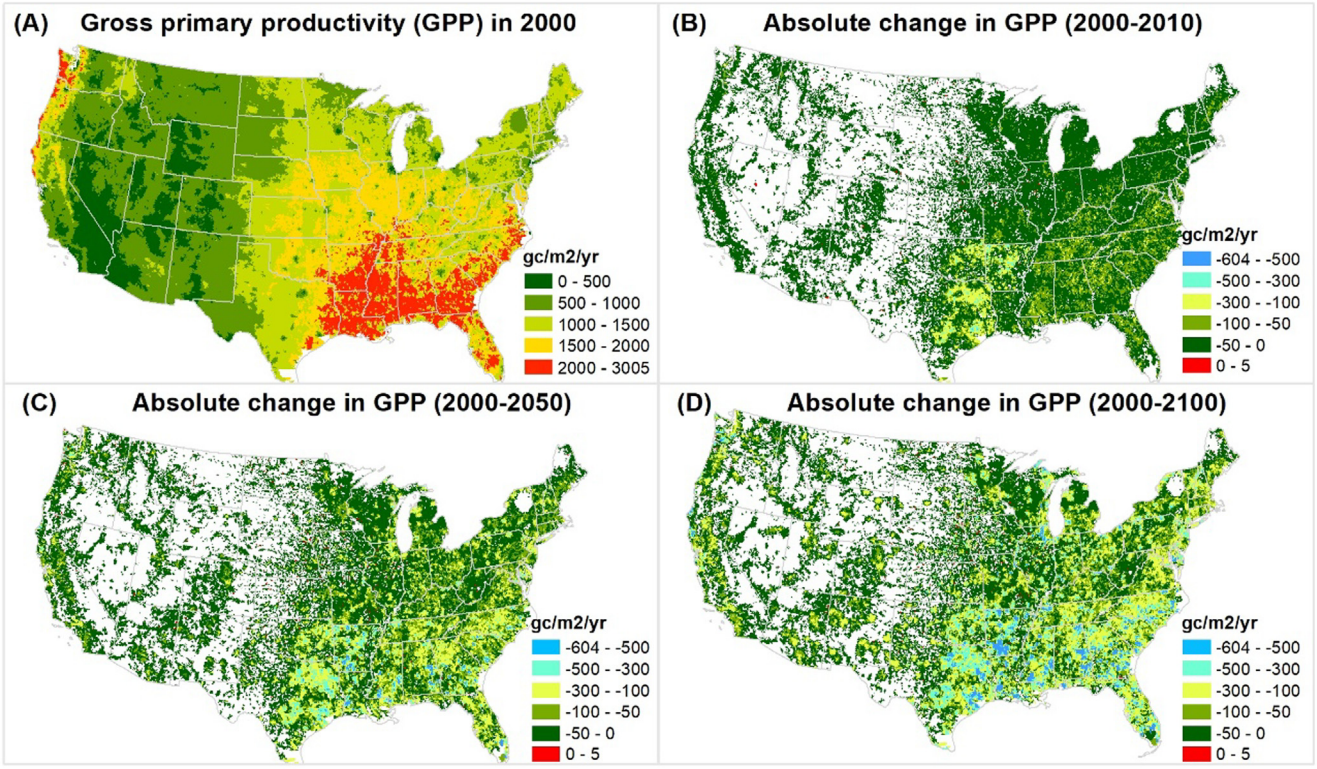

Fig. 4. Simulated gross primary productivity (GPP) in 2000 (A) and the absolute change in GPP during 2000–2010 (B), 2000–2050 (C), and 2000–2100 (D) at HUC12 watershed scale. Blank means no urbanization.

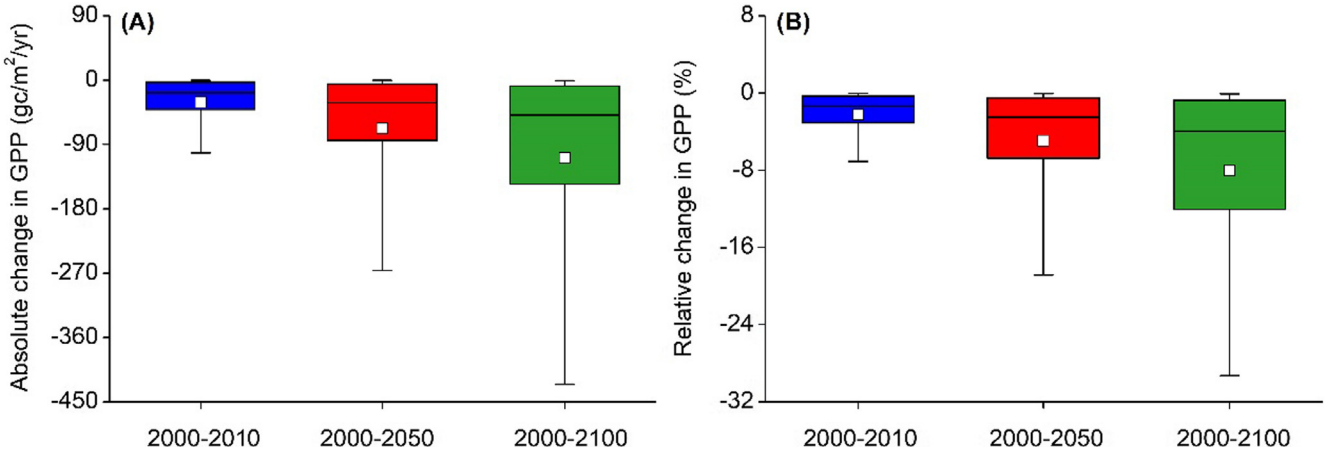

Fig. 5. The box-chart of absolute change (A) and relative change (B) in gross primary productivity (GPP) for 48,000–55,000 HUC12 watersheds impacted by urbanization during 2000–2100. The square is the mean value of the changes in GPP and the solid line is the median. The lower and upper whisker represents the 5th percentile and 95th percentile of the changes, respectively.

slope = −990–−650) than that in dry regions (R^2 = 0.78–0.94; slope = −547–−468) (Fig. 12, S5). As determined by the standardized stepwise regression coefficients, the magnitude of urbanization (i.e., changes in urban area) and the changes in grassland area were the two most influential factors controlling ΔGPP during the three time periods (Fig. 13, S6). In contrast, background climate and previous land cover types contributed little to ΔGPP.

3.5.2. GPP responses to urbanization as determined by the causal model

The IDA analysis showed that the changes in urban area from 2000 to 2050 (Urb0050) and grassland (Gras0050) were the direct causes of ΔGPP during 2000–2050 with the causal effect size of −3.72 and 0.55, respectively (Fig. 14). This means that when Urb0050 and Gras0050 increase or decrease by 1 standard unit, ΔGPP decreases or increases by 3.72 or 0.55 standard unit, respectively. Previous land use types of cropland (Crop00) and forest (For00) and changes in forest (For0050) were the indirect causes of ΔGPP with GPP changes with effect size of 0.06, −0.09 and 0.65, respectively. Although with directed edges to the dependent factor, historical climate of PPT and TEMP and changes in cropland (Crop0050) and impervious surface (IMP0050) were not considered as the causes of ΔGPP due to their small effect size of 0. Similarly, during 2000–2010, the land use change of Urb0010 and Gras0010 were the direct and indirect causes of ΔGPP with effect size of −1.76 and 0.94, respectively (Fig. S7). During 2000–2100, the land use change of Urb00100 was the direct cause of ΔGPP with effect size of −2.96 (Fig. S8). Previous land use types (Crop00, For00, Gras00, Shru00, Urb00) and land use change of Crop00100 and For00100 were the indirect causes with effect size ranged from −0.15 to 0.65 (Fig. S8).

4. Discussion

4.1. Complex interactions between responses of GPP and water to urbanization at the watershed scale

As expected, we found that ΔGPP closely followed the increase in urban area and the impacts varied across the CONUS over time. WaSSI appeared to be effective for projecting the negative impacts of urbanization on GPP, consistent with what were widely reported by previous individual studies (Diem et al., 2006; Imhoff et al., 2004; Seto et al., 2012; Trusilova and Churkina, 2008). The validation of the modeled GPP using the SIF product (Li and Xiao, 2019) showed that WaSSI reasonably captured GPP patterns under urbanization. The success was presumably because the WaSSI model considered the key controls on carbon and water balances including climate (water, energy) and vegetation (LAI, WUE) as identified in recent studies (Jenerette et al., 2009; Messori et al., 2019; P. Sun, 2019; Z.Y. Sun, 2019; Zhou and Xin,

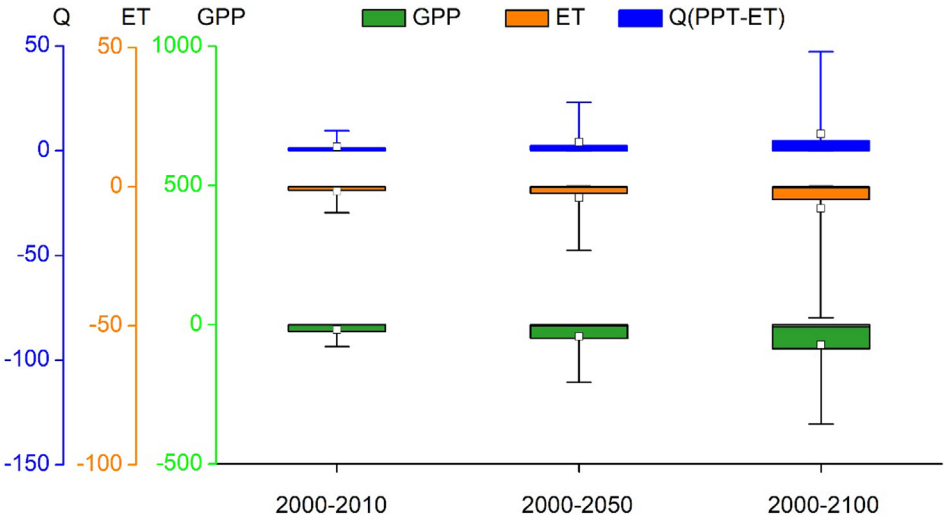

Fig. 6. Simulated mean changes in gross primary productivity (GPP) (g C m^{-2} yr^{-1}), evapotranspiration (ET) (mm yr^{-1}), and water yield (Q = Precipitation-ET) (mm yr^{-1}) for 48,000–55,000 HUC12 watersheds impacted by urbanization during 2000–2010, 2000–2050, and 2000–2100.

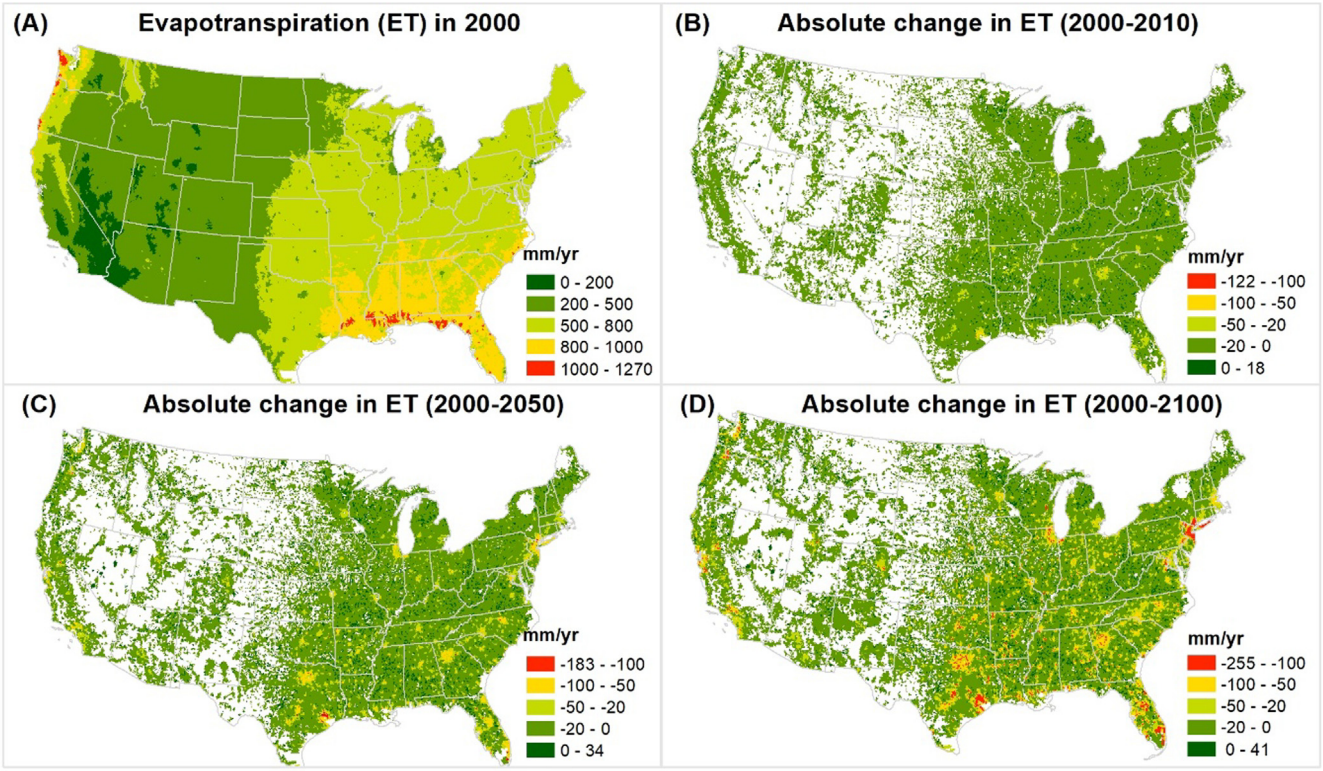

Fig. 7. Modeled annual evapotranspiration (ET) in 2000 (A) and the absolute change in ET during 2000–2010 (B), 2000–2050 (C), and 2000–2100 (D) at the HUC12 watershed scale.

2019). For example, Chen et al. (2019) identified precipitation, temperature and LAI as the three key drivers of ecosystem carbon fluxes at a global scale. As a water-centric model, WaSSI used the same three variables to estimate ET, a direct integrated variable, to estimate GPP. However, we found that urbanization caused an increase in GPP for 108–297 watersheds mainly in arid or semi-arid regions. Such results were coincided with findings of Zhao et al. (2007) and Buyantuyev and Wu (2009) who suggested that urbanization resulted in an increase in vegetation cover due to artificial greening.

Furthermore, we found that ΔGPP varied by watershed size, previous land use and cover types, and local climate. First, larger watersheds have larger ΔGPP than smaller ones, because larger watersheds can reduce more vegetation when the urban sprawl rate is equal (i.e., increase in urban area in each watershed area unit). However, the urbanization effects become more variable as the watersheds become smaller. Second, ΔGPP was more sensitive for watersheds dominated by wetlands, forest, cropland, and urban land. The probable reason was that high-water use efficiency (WUE) and change in ET for those land covers compared to grassland and shrubland. The changes in ET for wetlands is the highest among all the land uses due to their high levels of PET and large ET reduce capacity when converted to impervious surfaces (assumed to be close to zero in this study). Watersheds dominated by vegetation coverage with deep roots such as forest, generally have higher evapotranspiration rates (ET/PPT) (Deng et al., 2015; Li et al., 2018b), and the changes in ET is relatively high compared to other land use conversions. In addition, different land uses have various WUE (Cropland > Forest > Grassland > Shrubland, Savanas, and Wetland) (Sun et al., 2011b). Thus, watersheds dominated by wetland, forest, and cropland would have higher change in WUE or ET, therefore ΔGPP, as a result of urban area expansion. Similarly, urban dominated

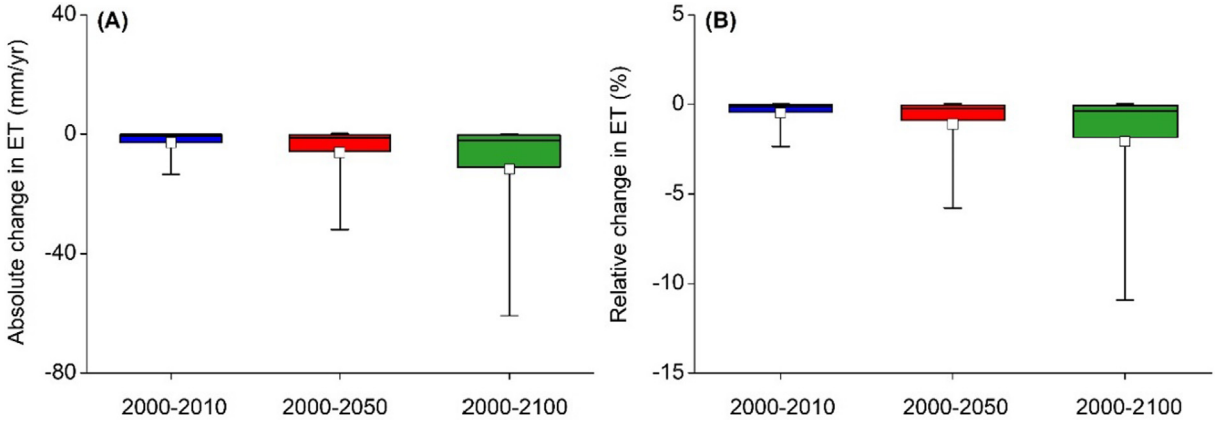

Fig. 8. The box-chart of absolute change (A) and relative change (B) in evapotranspiration (ET) for 48,000–55,000 HUC12 watersheds impacted by urbanization during 2000–2100. The square is the mean value of the changes in ET and the solid line is the median. The lower and upper whisker represents the 5th percentile and 95th percentile of the changes, respectively.

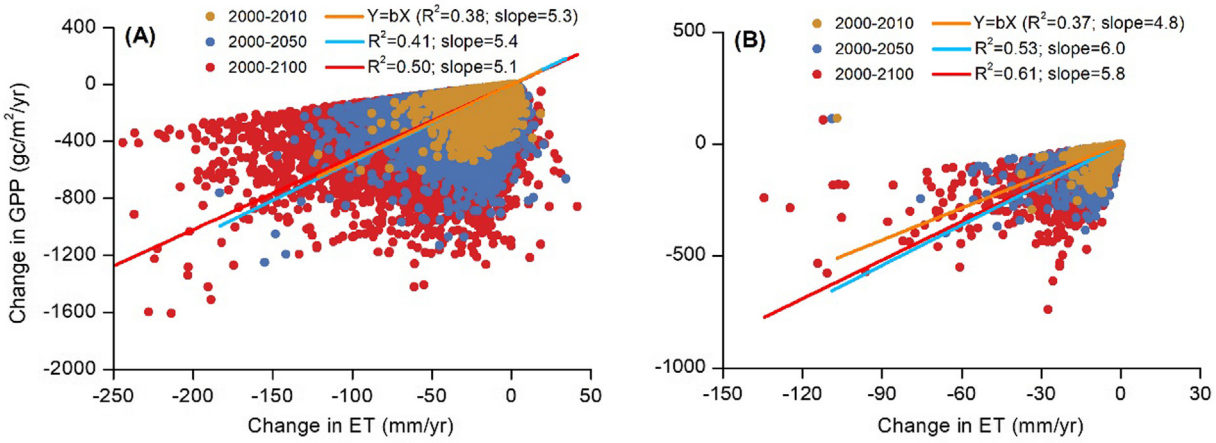

Fig. 9. Linear regression of the change in gross primary productivity (GPP) to change in evapotranspiration (ET) during 2000–2010, 2000–2050 and 2000–2100 at both HUC12 (A) and HUC8 (B) scale.

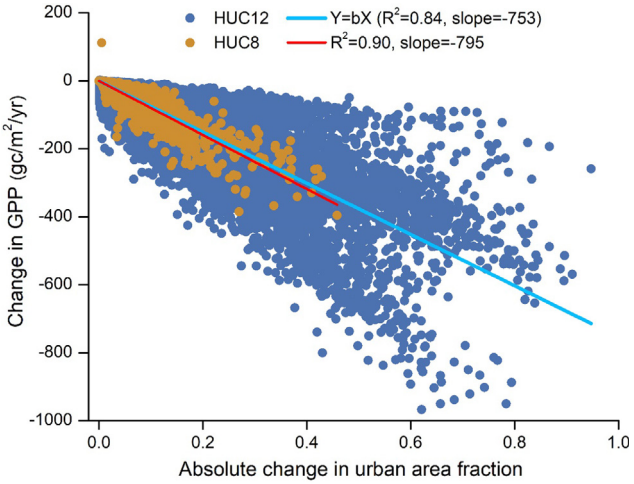

Fig. 10. Scatter plot to show relationship between the absolute change in gross primary productivity (GPP) and the absolute change in urban area fraction during 2000–2050 at both HUC12 and 8-digit Hydrologic Unit Code (HUC8) watershed scales.

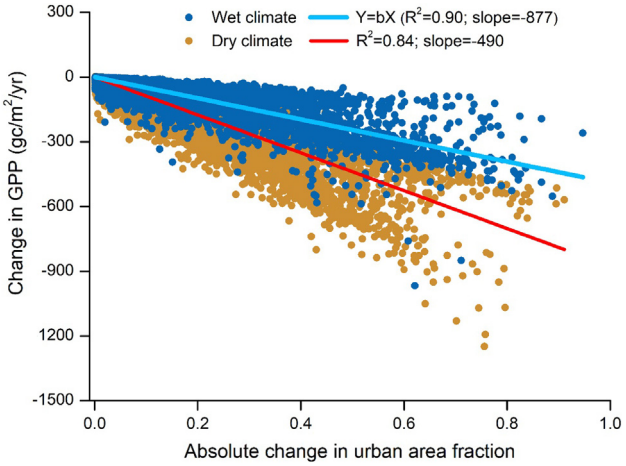

Fig. 12. Scatter plot to show relationship between the change in gross primary productivity (GPP) to the absolute change in impervious surface for both wet (PPT/PET > = 1) and dry (PPT/PET < 1) climate during 2000–2050. PPT and PET denote precipitation and potential evapotranspiration, respectively.

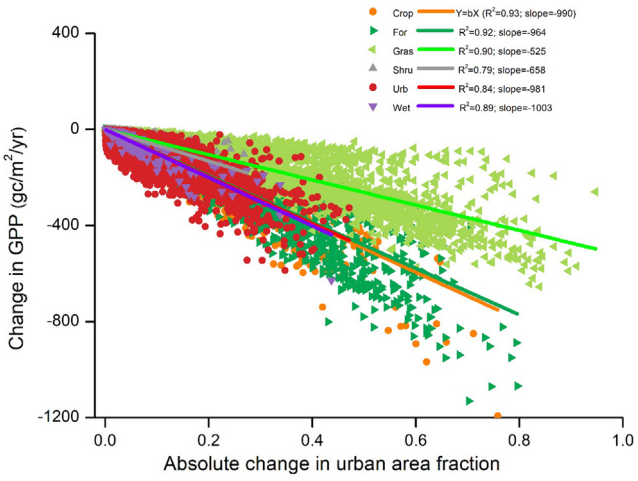

Fig. 11. Scatter plot to show relationship between the change in gross primary productivity (GPP) and the absolute change in urban area fraction during 2000–2050 for watersheds previously dominated by forest, urban, shrubland, grassland, cropland, water and wetland lands of the base year 2000 at HUC12 scale.

watersheds generally have greater urban area growth rates than non-urban (i.e., forest, shrubland, and grassland) dominated watersheds, and thus have larger ΔGPP when removing vegetations by urbanization. Previous studies also found that hydrological responses of urban dominated watersheds were more sensitive to urbanization than the non-urban dominated watersheds (Kumar et al., 2018; Putro et al., 2016; Rouge and Cai, 2014). Third, ΔGPP in wet regions was more sensitive to urbanization due to large coverages of forest and wetland in wet regions. Wet and forested areas had large changes in WUE and ET when they were converted to other land uses. All these results support a previous study conclusion that urbanization effects varied by vegetation type and biome (Miller et al., 2018).

The ΔGPP at the watershed scale did not linearly follow the ET changes by LULC as originally surmised. The main reason was that the WUE (GPP/ET) differed among land cover types (Ekness and Randhir, 2015; Li et al., 2018a; Sun et al., 2011b) and the watershed land use compositions including impervious surface fraction patters were complex, resulting in a nonlinear relationship between ET and GPP at the watershed level. The complex interactions between carbon and water at a large scale was also noted in Cheng et al. (2017). They found that the changes in terrestrial carbon uptake did not proportionally follow the changes in ET but rather followed changes in WUE. However, the inter-annual ET-GPP coupling in semi-arid regions appeared to be rather high (Biederman et al., 2016; Zhang et al., 2016b).

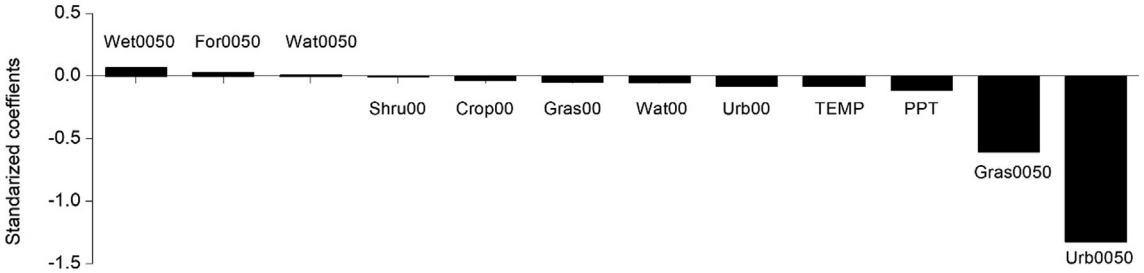

Fig. 13. Standardized stepwise regression coefficients of the change in gross primary productivity (GPP) to the selected controlling factors during 2000–2050 at HUC12 watershed scale.

4.2. Urbanization impacts across time and space

Our modeling analysis suggested that both the previous land cover characteristics, and historical climate and land cover changes influenced ΔGPP through time, which supported Hypothesis #2. Among these controlling factors, changes in urban area and grassland played the most important role. However, correlation does not necessarily imply causation. The IDA results further demonstrated that urban area growth was the direct cause of the changes in GPP through time. In contrast, previous LULCC of non-urban lands were identified as indirect causes of ΔGPP. In general, our findings are consistent with previous individual studies (Buyantuyev and Wu, 2009; Diem et al., 2006; Imhoff et al., 2004; Seto et al., 2012; Trusilova and Churkina, 2008). The present study represents a novel integration of various findings at a national scale.

4.3. Implications for watershed ecosystem management

This study suggested that that there was a tradeoff between water yield and GPP. Reduction in ecosystem GPP may cause concerns of organic matter inputs to urban aquatic ecosystems and thus negatively affect fauna habitats, biodiversity, and aquatic ecosystem productivity

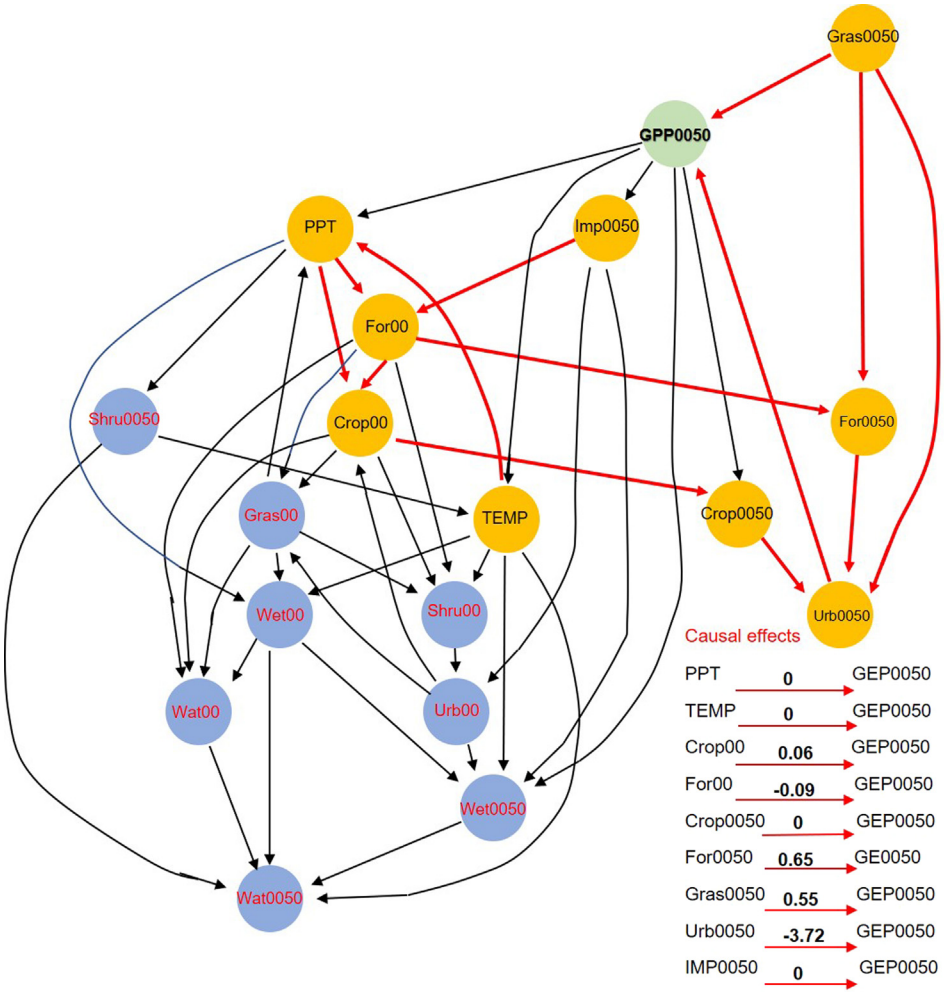

Fig. 14. Causal networks and causal effects among change in gross primary productivity (GPP0050; green circle) and the controlling factors (blue and orange circles) during 2000–2050 derived from IDA. Orange circles denote controlling factors which are causally related to water yield change and red directed edges denote the causal relations. The causal relations and effect (in numbers) are shown at the right corner of each network. (For interpretation of the references to colour in this figure legend, the reader is referred to the web version of this article.)

(Sun and Lockaby, 2012). The increase of water yield from a watershed can be beneficial (i.e., reduced water stress) or harmful (increased overland flow and stormflow, erosion and sedimentation). At the national scale, carbon–water tradeoffs should be considered in developing policies for reducing carbon emission and maintaining stream water supply and water quality. For example, similar to previous findings (Boggs and Sun, 2011) and (Oudin et al., 2018), the WRR03, WRR06, WRR08 and WRR12 in the wet regions in the southeastern U.S. are projected to have pronounced increase in water yield but large decrease in GPP. However, the amplification of water quantity by urbanization often causes water quality problems and cautions are needed to consider the likely negative effects of GPP decline (Sun and Lockaby, 2012). Maintaining forest coverage and thus GPP during urbanization in the watersheds in southeastern U.S. is essential to mitigate the negative impacts of urbanization on watershed ecosystem health. Forest maintenance and restoration is a way in preventing a drastic decrease in GPP (Nuarsa et al., 2018). One important finding from this study and others (Miller et al., 2018) was that the impacts of urbanization on GPP varied among watersheds under different climate and watershed characteristics (i.e., previous land cover type, and land use and cover changes). Therefore, effective integrated watershed management strategies must be designed to fit local climatic and watershed conditions.

4.4. Uncertainty

As for any modeling results, uncertainty comes from both the model itself and from input data driving the model (Xiao et al., 2014a; Zheng et al., 2018). The WaSSI model algorithms for estimating GPP is biome based. Unfortunately, very few urban flux sites existed and GPP and ET data are limited to derive urban ecosystem WUE. In this study, we lumped three types of forest (i.e., deciduous forest, evergreen forest, mixed forest) into one category of forest due to the limitation of ICLUS data. We set the same impervious fraction and LAI values per land use of the three subtypes of forest. Thus, GPP reported here may have bias for some watersheds, either overestimated or underestimated.

The uncertainty of models could be reduced by improving model inputs such as refined land use and cover and MODIS-based LAI datasets. As demonstrated by other studies (Kimball et al., 2018), refined land cover and climate dataset inputs increased the accuracy of MODIS-based GPP estimates. Similarly, improved climate data for urban areas will improve modeling result accuracy.

Climate is a key factor controlling ET and GPP at a broad scale (Chen et al., 2019; Messori et al., 2019) and confirmed by the current study. However, this study mainly focused on the sensitivity of urbanization assuming a static climate conditions through time. Future climate change including the rise of CO_2 concentration is likely to affect vegetation dynamics and carbon fixation (Golladay et al., 2016; Sun et al., 2018; Wang et al., 2018a), ET, WUE, and GPP. However, the climate change projections are highly uncertain and its impacts on ecosystem structure and functions are extremely variable (Mankin et al., 2019). Precipitation was found to exert positive impacts on ecosystem productivity in semiarid regions, while warming may have negative effects (Zhao et al., 2019). The impacts of climate change and other factors such as nitrogen deposition, CO_2 fertilization, and urban heat island effects on WUE remains controversial (Mankin et al., 2019).

Future global climate change and local urban meteorological change such as 'Urban Heat Island (Zhou et al., 2019) or 'Urban Dry Island' (Hao et al., 2018) may overwhelm the LULCC effects on water fluxes as recently demonstrated by Martin et al. (2017). At a global scale, climate factors including rising CO_2, temperature and water conditions generally had positive impacts on GPP. Sun et al. (2018) demonstrated that LULCC had a negative impact on global GPP, especially in regions with high rates of forest loss, which is consistent with our findings. Thus, climate change and LULCC driven by urbanization are often coupled, and they should be addressed together to fully quantify the tradeoffs between GPP loss and water yield rise in watersheds.

5. Conclusions

The effects of urbanization on gross primary productivity (GPP) and water yield across the continental United States (CONUS) were quantified by integrating a water-centric ecosystem model (WaSSI), historical climate (1961–2010) and both historical, and projected future LULCC at both 12-digit and 8-digit Hydrologic Unit Code watershed scales. We found that the total amount of CONUS carbon uptake decreased through time and varied across space. Watersheds with a large decrease in GPP were found in warm and wet regions of the southeastern U.S., overlapped with regions of large water production. The trade-offs and coupling between carbon and water fluxes (i.e., GPP, ET, water yield) at the watershed level were complex, and were affected by climate, vegetation structure, and watershed landcover compositions. In addition, the impacts of urbanization on GPP varied among watersheds with different background climate, previous land cover types, and the magnitude of LULCC. LULCC, especially urban growth in watershed dominated by urban uses, played the most important role in controlling the variations of GPP in future periods.

Water and carbon fluxes are closely coupled, and our study supports the hypothesis that "GPP responses to urbanization vary across the space" through time as affected by water and energy availability. We conclude that effective environmental management measures and strategies must be designed to fit regional and local watershed conditions. To reduce impacts of urbanization on ecosystems including terrestrial and aquatic components of the watersheds, it is important to maintain vegetation covers and hydrological functions in urbanizing watersheds through conserving forests and wetlands or developing other 'green infrastructure'.

The current study examined the GPP sensitivity to potential urbanization at the CONCUS scale and how this potential change interacted with water availability (i.e. the balance of precipitation and ET). Our study provides a benchmark on the likely impacts of urbanization alone on ecosystem water and carbon fluxes. Future studies should evaluate urbanization effects under a changing climate because urbanization may aggravate or offset the effects of climate change on GPP depending on future climate and management conditions.

CRediT authorship contribution statement

Cheng Li: Writing - original draft, Formal analysis. **Ge Sun:** Conceptualization, Supervision, Writing - review & editing. **Erika Cohen:** Methodology. **Yindan Zhang:** Methodology. **Jingfeng Xiao:** Writing - review & editing. **Steven G. McNulty:** Writing - review & editing. **Ross K. Meentemeyer:** Writing - review & editing.

Declaration of Competing Interest

The authors declare that they have no known competing financial interests or personal relationships that could have appeared to influence the work reported in this paper.

Acknowledgements

This study was supported by the U.S. Department of Agriculture Forest Service. The Authors would like to thank two anonymous reviewer and associate editor for their suggestions that improved the original manuscript. Data are available upon request from the corresponding author.

Appendix A. Supplementary data

Supplementary data to this article can be found online at https://doi.org/10.1016/j.jhydrol.2020.124581.

References

As-syakur, A.R., Osawa, T., Adnyana, I.W.S., 2010. Medium spatial resolution satellite imagery to estimate gross primary production in an urban area. Remote Sens. 2 (6), 1496–1507. https://doi.org/10.3390/rs2061496.

Awal, M.A., et al., 2010. Comparing the carbon sequestration capacity of temperate deciduous forests between urban and rural landscapes in central Japan. Urban For. Urban Gree. 9 (3), 261–270. https://doi.org/10.1016/j.ufug.2010.01.007.

Bagstad, K.J., Cohen, E., Ancona, Z.H., McNulty, S., Sun, G., 2018. Testing data and model selection effects for ecosystem service assessment in Rwanda. Appl. Geography 93, 25–36.

Beer, C., Reichstein, M., Ciais, P., Farquhar, G.D., Papale, D., 2007. Mean annual GPP of Europe derived from its water balance. Geophys. Res. Lett. 34L05401. https://doi.org/10.1029/2006GL029006.

Beer, C., et al., 2010. Terrestrial gross carbon dioxide uptake: global distribution and covariation with climate. Science 329, 834–838.

Biederman, J., et al., 2016. Terrestrial carbon balance in a drier world: the effects of water availability in southwestern North America. Global Change Biol. 22, (5). https://doi.org/10.1111/gcb.13222.

Boggs, J., Sun, G., 2011. Urbanization alters watershed hydrology in the Piedmont of North Carolina. Ecohydrology 4, 256–264.

Buyantuyev, A., Wu, J.G., 2009. Urbanization alters spatiotemporal patterns of ecosystem primary production: a case study of the Phoenix metropolitan region, USA. J. Arid Environ. 73 (4–5), 512–520.

Caldwell, P.V., Sun, G., McNulty, S.G., Cohen, E.C., Myers, J.A.M., 2012. Impacts of impervious cover, water withdrawals, and climate change on river flows in the conterminous US. Hydrol. Earth Syst. Sci. 16 (8), 2839–2857. https://doi.org/10.5194/hess-16-2839-2012.

Chapin III, F.S., Matson, P.A., Mooney, H.A., 2002. Principles of Terrestrial Ecosystem Ecology. Springer, Berlin.

Chen, S., Zou, J., Hu, Z., Lu, Y., 2019. Climate and vegetation drivers of terrestrial carbon fluxes: a global data synthesis. Adv. Atmos. Sci. 36 (7), 679–696. https://doi.org/10.1007/s00376-019-8194-y.

Cheng, L., et al., 2017. Recent increases in terrestrial carbon uptake at little cost to the water cycle. Nat. Commun. 8. https://doi.org/10.1038/s41467-017-00114-5.

Churkina, G., 2008. Modeling the carbon cycle of urban systems. Ecol. Modell. 216 (2), 107–113.

Cui, Y.P., et al., 2017. Temporal consistency between gross primary production and solarinduced chlorophyll fluorescence in the ten most populous megacity areas over years. Sci. Rep. 7. https://doi.org/10.1038/s41598-017-13783-5.

Deng, X.Z., Shi, Q.L., Zhang, Q., Shi, C.C., Yin, F., 2015. Impacts of land use and land cover changes on surface energy and water balance in the Heihe River Basin of China, 2000–2010. Phys. Chem. Earth 79–82, 2–10. https://doi.org/10.1016/j.pce.2015.01.002.

Diem, J., Ricketts, C.E., Dean, J.R., 2006. Impacts of urbanization on land-atmosphere carbon exchange within a metropolitan area in the USA. Clim. Res. 30, 201–213. https://doi.org/10.3354/cr030201.

Duan, K., et al., 2016. Divergence of ecosystem services in US National Forests and Grasslands under a changing climate. Sci. Rep. 6. https://doi.org/10.1038/srep24441.

Ekness, P., Randhir, T.O., 2015. Effect of climate and land cover changes on watershed runoff: a multivariate assessment for storm water management. J. Geophys. Res.: Biogeosci. 120 (9), 1785–1796. https://doi.org/10.1002/2015jg002981.

Finzi, A.C., Cole, J.J., Doney, S.C., Holland, E.A., Jackson, R.B., 2011. Research frontiers in the analysis of coupled biogeochemical cycles. Front. Ecol. Environ. 9 (1), 74–80. https://doi.org/10.1890/100137.

Gitelson, A.A., Peng, Y., Arkebauer, T.J., Schepers, J., 2014. Relationships between gross primary production, green LAI, and canopy chlorophyll content in maize: implications for remote sensing of primary production. Remote Sens. Environ. 144, 65–72. https://doi.org/10.1016/j.rse.2014.01.004.

Golladay, S.W., et al., 2016. Achievable future conditions as a framework for guiding forest conservation and management. Forest Ecol. Manage. 360 (17), 80–96.

Grace, J.B., 2006. Structural Equation Modeling and Natural Systems. Cambridge University Press, New York, US, pp. 361.

Grimm, N.B., et al., 2008. Global change and the ecology of cities. Science 319 (5864), 756–760.

Hao, L., et al., 2018. Ecohydrological processes explain urban dry island effects in a wet region, Southern China. Water Resour. Res. 54 (9), 6757–6771. https://doi.org/10.1029/2018wr023002.

Imhoff, M., et al., 2004. The consequences of urban land transformation on net primary productivity in the United States. Remote Sens. Environ. 89, 434–443. https://doi.org/10.1016/j.rse.2003.10.015.

Jenerette, G.D., Scott, R.L., Barron-Gafford, G.A., Huxman, T.E., 2009. Gross primary production variability associated with meteorology, physiology, leaf area, and water supply in contrasting woodland and grassland semiarid riparian ecosystems. J. Geophys. Res.: Biogeo. 114. https://doi.org/10.1029/2009jg001074.

Jung, M., et al., 2017. Compensatory water effects link yearly global land CO_2 sink changes to temperature. Nature 541, 516. https://doi.org/10.1038/nature20780.

Kalisch, M., Bühlmann, P., 2007. Estimating high-dimensional directed acyclic graphs with the PC-algorithm. J. Machine Learn. Res. 8 (5), 613–636.

Kalisch, M., Mächler, M., Colombo, D., Maathuis, M.H., Bühlmann, P., 2012. Causal inference using graphical models with the R Package pcalg. J. Stat. Softw. 47 (11), 26. https://doi.org/10.18637/jss.v047.i11.

Kimball, H.L., Selmants, P.C., Moreno, A., Running, S.W., Giardina, C.P., 2018. Evaluating the role of land cover and climate uncertainties in computing gross primary production in Hawaiian Island ecosystems. Plos One 13 (1). https://doi.org/10.1371/journal.pone.0192041.

Kumar, S., Moglen, G.E., Godrej, A.N., Grizzard, T.J., Post, H.E., 2018. Trends in water yield under climate change and urbanization in the US Mid-Atlantic region. J. Water Resour. Plan. Manage. -ASCE, 144(8). doi: 0501800910.1061/(asce)wr.1943-5452.0000937.

Law, B.E., et al., 2002. Environmental controls over carbon dioxide and water vapor exchange of terrestrial vegetation. Agr. Forest Meteorol. 113 (1), 97–120. https://doi.org/10.1016/S0168-1923(02)00104-1.

Lei, H.M., et al., 2014. Sensitivity of global terrestrial gross primary production to hydrologic states simulated by the Community Land Model using two runoff parameterizations. J. Adv. Model. Earth Sy. 6 (3), 658–679. https://doi.org/10.1002/2013ms000252.

Li, J., et al., 2018a. Response of net primary production to land use and land cover change in mainland China since the late 1980s. Sci. Total Environ. 639, 237–247. https://doi.org/10.1016/j.scitotenv.2018.05.155.

Li, S.X., Yang, H., Lacayo, M., Liu, J.G., Lei, G.C., 2018b. Impacts of land-use and land-cover changes on water yield: a case study in Jing-Jin-Ji, China. Sustainability 10(4). doi: 96010.3390/su10040960.

Li, X., et al., 2018c. Solar-induced chlorophyll fluorescence is strongly correlated with terrestrial photosynthesis for a wide variety of biomes: first global analysis based on OCO-2 and flux tower observations. Global Change Biol. 24 (9), 3990–4008. https://doi.org/10.1111/gcb.14297.

Li, X., Xiao, J., 2019. A global, 0.05-degree product of solar-induced chlorophyll fluorescence derived from OCO-2, MODIS, and reanalysis data. Remote Sens. 11 (5), 517.

Liu, N., et al., 2018a. Parallelization of a distributed ecohydrological model. Environ. Modell. Softw. 101, 51–63. https://doi.org/10.1016/j.envsoft.2017.11.033.

Liu, N., Sun, P.S., Liu, S.R., Sun, G., 2013. Coupling simulation of water-carbon processes for catchment-calibration and validation of the WaSSI-C model. Chin. J. Plant Ecol. 37 (6), 492–502 (in Chinese).

Liu, S.S., Du, W., Su, H., Wang, S.Q., Guan, Q.F., 2018b. Quantifying impacts of land-use/cover change on urban vegetation gross primary production: a case study of Wuhan, China. Sustainability 10 (3). https://doi.org/10.3390/su10030714.

Liu, Y., et al., 2017. Causal inference between bioavailability of heavy metals and environmental factors in a large-scale region. Environ. Pollut. 226, 370–378.

Liu, Z.F., He, C.Y., Zhou, Y.Y., Wu, J.G., 2014. How much of the world's land has been urbanized, really? A hierarchical framework for avoiding confusion. Landscape Ecol. 29 (5), 763–771.

Maathuis, M.H., Colombo, D., Kalisch, M., Bühlmann, P., 2010. Predicting causal effects in large-scale systems from observational data. Nat. Methods 7, 247–248. https://doi.org/10.1038/nmeth0410-247.

Martin, K.L., et al., 2017. Watershed impacts of climate and land use changes depend on magnitude and land use context. Ecohydrology 10 (7), e1870. https://doi.org/10.1002/eco.1870.

Mankin, J.S., Seager, R., Smerdon, J.E., Williams, A.P., Cook, B.I., 2019. Mid-latitude freshwater availability reduced by projected vegetation responses to climate change. Nat. Geosci. doi: 10.1038/s41561-019-0480-x.

McHale, M.R., Hall, S.J., Majumdar, A., Grimm, N.B., 2017. Carbon lost and carbon gained: a study of vegetation and carbon trade-offs among diverse land uses in Phoenix, Arizona. Ecol. Appl. 27 (2), 644–661. https://doi.org/10.1002/eap.1472.

Messori, G., Ruiz-Pérez, G., Manzoni, S., Vico, G., 2019. Climate drivers of the terrestrial carbon cycle variability in Europe. Environ. Res. Lett. 14 (6), 063001. https://doi.org/10.1088/1748-9326/ab1ac0.

Miller, D.L., et al., 2018. Gross primary productivity of a large metropolitan region in midsummer using high spatial resolution satellite imagery. Urban Ecosyst. 21 (5), 831–850. https://doi.org/10.1007/s11252-018-0769-3.

Mo, X.G., Liu, S.X., Chen, X., Hu, S., 2018. Variability, tendencies, and climate controls of terrestrial evapotranspiration and gross primary productivity in the recent decade over China. Ecohydrology 11 (4). https://doi.org/10.1002/eco.1951.

Monteith, J.L., 1972. Solar radiation and productivity in tropical ecosystems. J. Appl. Ecol. 9, 747766. https://doi.org/10.2307/2401901.

Morgan, S.L., 2013. Handbook of Causal Analysis for Social Research. Springer, New York.

Nuarsa, I.W., As-Syakur, A., Gunadi, I.G.A., Sukewijaya, I.M., 2018. Changes in Gross Primary Production (GPP) over the Past Two Decades Due to Land Use Conversion in a Tourism City. ISPRS Int. J. Geo.-Inf. 7(2). doi: 10.3390/ijgi7020057.

Oudin, L., Salavati, B., Furusho-Percot, C., Ribstein, P., Saadi, M., 2018. Hydrological impacts of urbanization at the catchment scale. J. Hydrol. 559, 774–786. https://doi.org/10.1016/j.jhydrol.2018.02.064.

Pearl, J., 1995. Causal diagrams for empirical research. Biometrika 82, 669–688.

Pearl, J., 2003. Causality: models, reasoning and inference. Economet. Theor. 19, 675–685.

Potter, C.S., et al., 1993. Terrestrial ecosystem production: a process model based on global satellite and surface data. Global Biogeochem. Cy. 7, 811–841.

Proietti, C., et al., 2019. A new wetness index to evaluate the soil water availability influence on gross primary production of European forests. Climate 7(3). doi: 10.3390/cli7030042.

Putro, B., Kjeldsen, T.R., Hutchins, M.G., Miller, J., 2016. An empirical investigation of climate and land-use effects on water quantity and quality in two urbanising catchments in the southern United Kingdom. Sci. Total Environ. 548, 164–172. https://doi.org/10.1016/j.scitotenv.2015.12.132.

Romero-Lankao, P., et al., 2014. A critical knowledge pathway to low-carbon, sustainable futures: integrated understanding of urbanization, urban areas, and carbon. Earths Future 2 (10), 515–532. https://doi.org/10.1002/2014ef000258.

Rouge, C., Cai, X.M., 2014. Crossing-scale hydrological impacts of urbanization and climate variability in the Greater Chicago Area. J. Hydrol. 517, 13–27. https://doi.org/

10.1016/j.jhydrol.2014.05.005.
Running, S.W., Zhao, M.S., 2015. Daily GPP and annual NPP (MOD17A2/A3) products NASA earth observing system MODIS land algorithm. MOD17 User's Guide.
Seto, K.C., Guneralp, B., Hutyra, L.R., 2012. Global forecasts of urban expansion to 2030 and direct impacts on biodiversity and carbon pools. Proc. Natl. Acad. Sci. U.S.A. 109 (40), 16083–16088. https://doi.org/10.1073/pnas.1211658109.
Sun, G., et al., 2011a. A general predictive model for estimating monthly ecosystem evapotranspiration. Ecohydrology 4 (2), 245–255. https://doi.org/10.1002/eco.194.
Sun, G., et al., 2011b. Upscaling key ecosystem functions across the conterminous United States by a water-centric ecosystem model. J. Geophys. Res. 116 (G00J05), 1–16.
Sun, G., Caldwell, P.V., McNulty, Steven G., 2015a. Modeling the potential role of forest thinning in maintaining water supplies under a changing climate across the Conterminous United States. Hydrol. Process. 29 (24). https://doi.org/10.1002/hyp.10469.
Sun, G., Lockaby, B.G., 2012. Water quantity and quality at the urbanrural interface. In: Laband, D.N., Lockaby, B.G., Zipperer, W. (Eds.), Urban-rural Interfaces: Linking People and Nature. American Society of Agronomy, Crop Science Society of America, Soil Science Society of America, Madison, Wisconsin.
Sun, P., et al., 2019a. Remote sensing and modeling fusion for investigating the ecosystem water-carbon coupling processes. Sci. Total Environ. 697, 134064. https://doi.org/10.1016/j.scitotenv.2019.134064.
Sun, S., et al., 2016. Projecting water yield and ecosystem productivity across the United States by linking an ecohydrological model to WRF dynamically downscaled climate data. Hydrol. Earth Syst. Sc. 20 (2), 935–952. https://doi.org/10.5194/hess-20-935-2016.
Sun, S.L., et al., 2015b. Drought impacts on ecosystem functions of the U.S. National Forests and Grasslands: Part I. Evaluation of a water and carbon balance model. Forest Ecol. Manage. 353, 260–268.
Sun, S.L., et al., 2015c. Drought impacts on ecosystem functions of the U.S. National Forests and Grasslands: Part II Model results and management implications. Forest Ecol. Manage. 353, 269–279.
Sun, Z.Y., et al., 2018. Spatial pattern of GPP variations in terrestrial ecosystems and its drivers: climatic factors, CO_2 concentration and land-cover change, 1982–2015. Ecol. Inform. 46, 156–165. https://doi.org/10.1016/j.ecoinf.2018.06.006.
Sun, Z.Y., et al., 2019b. Evaluating and comparing remote sensing terrestrial GPP models for their response to climate variability and CO_2 trends. Sci. Total Environ. 668, 696–713. https://doi.org/10.1016/j.scitotenv.2019.03.025.
Trusilova, K., Churkina, G., 2008. The response of the terrestrial biosphere to urbanization: land cover conversion, climate, and urban pollution. Biogeosciences 5, 2445–2470. https://doi.org/10.5194/bgd-5-2445-2008.
U.S. EPA (U.S. Environmental Protection Agency). 2017. Integrated Climate and Land-Use Scenarios (ICLUS version 2.1) for the Fourth National Climate Assessment. Available at: https://www.epa.gov/iclus.
Wang, M.M., et al., 2018a. Detection of positive gross primary production extremes in terrestrial ecosystems of China during 1982–2015 and analysis of climate contribution. J. Geophy. Res.-Biogeo. 123 (9), 2807–2823. https://doi.org/10.1029/2018jg004489.
Wang, Q., Liu, J., Chen, Z., Li, F., Yu, H., 2018b. A causation-based method developed for an integrated risk assessment of heavy metals in soil. Sci. Total Environ. 642, 1396–1405.
Wu, J., 2014. Urban ecology and sustainability: the state-of-the-science and future directions. Landscape Urban Plan. 125, 209–221.
Wu, Y., Liu, S., Qiu, L., Sun, Y., 2016. SWAT-DayCent coupler: an integration tool for simultaneous hydro-biogeochemical modeling using SWAT and DayCent. Environ. Modell. Softw. 86, 81–90. https://doi.org/10.1016/j.envsoft.2016.09.015.
Xiao, J., et al., 2008. Estimation of net ecosystem carbon exchange for the conterminous United States by combining MODIS and AmeriFlux data. Agr. Forest Meteorol. 148 (11), 1827–1847. https://doi.org/10.1016/j.agrformet.2008.06.015.
Xiao, J., et al., 2011. Assessing net ecosystem carbon exchange of U.S. terrestrial ecosystems by integrating eddy covariance flux measurements and satellite observations. Agr. Forest Meteorol. 151 (1), 60–69. https://doi.org/10.1016/j.agrformet.2010.09.002.
Xiao, J., et al., 2010. A continuous measure of gross primary production for the conterminous United States derived from MODIS and AmeriFlux data. Remote Sens. Environ. 114 (3), 576–591. https://doi.org/10.1016/j.rse.2009.10.013.
Xiao, J., Davis, K.J., Urban, N.M., Keller, K., 2014a. Uncertainty in model parameters and regional carbon fluxes: a model-data fusion approach. Agr. Forest Meteorol. 189–190, 175–186. https://doi.org/10.1016/j.agrformet.2014.01.022.
Xiao, J., et al., 2014b. Data-driven diagnostics of terrestrial carbon dynamics over North America. Agr. Forest Meteorol. 197, 142–157. https://doi.org/10.1016/j.agrformet.2014.06.013.
Zhang, Y., et al., 2016a. Development of a coupled carbon and water model for estimating global gross primary productivity and evapotranspiration based on eddy flux and remote sensing data. Agr. Forest Meteorol. 223, 116–131.
Zhang, Y., et al., 2016b. Precipitation and carbon-water coupling jointly control the interannual variability of global land gross primary production. Sci. Rep. 6. https://doi.org/10.1038/srep39748.
Zhao, M.S., Heinsch, F.A., Nemani, R.R., Running, S.W., 2005. Improvements of the MODIS terrestrial gross and net primary production global data set. Remote Sens. Environ. 95 (2), 164–176.
Zhao, T.T., Brown, D.G., Bergen, K.M., 2007. Increasing gross primary production (GPP) in the urbanizing landscapes of southeastern Michigan. Photogramm. Eng. Rem. S. 73 (10), 1159–1167. https://doi.org/10.14358/pers.73.10.1159.
Zhao, F., et al., 2019. Climatic and hydrologic controls on net primary production in a semiarid loess watershed. J. Hydrol., 568, 803–815. doi: 10.1016/ j.jhydrol.2018.11.031.
Zheng, Y., et al., 2018. Sources of uncertainty in gross primary productivity simulated by light use efficiency models: model structure, parameters, input data, and spatial resolution. Agr. Forest Meteorol. 263, 242–257. https://doi.org/10.1016/j.agrformet.2018.08.003.
Zhou, D., et al., 2019. Satellite remote sensing of surface urban heat islands: progress, challenges, and perspectives. Remote Sens. 11 (1), 48.
Zhou, X.W., Xin, Q.C., 2019. Improving satellite-based modelling of gross primary production in deciduous broadleaf forests by accounting for seasonality in light use efficiency. Int. J. Remote Sens. 40 (3), 931–955. https://doi.org/10.1080/01431161.2018.1519285.